Macroscopic lamellar heterophase pattern in $Pb(Mg_{1/3}Nb_{2/3})O_3$-$PbTiO_3$ single crystals

I. Rafalovskyi,[1] M. Guennou,[1,2] I. Gregora,[1] and J. Hlinka[1,*]

[1]*Institute of Physics, The Czech Academy of Sciences, Na Slovance 2, 182 21 Prague 8, Czech Republic*

[2]*Materials Research and Technology Department, Luxembourg Institute of Science and Technology, 41 rue du Brill, L-4422 Belvaux, Luxembourg*

(Received 26 March 2013; revised manuscript received 17 December 2015; published 16 February 2016)

The paper describes lamellar heterostructures, observed in $(1-x)Pb(Mg_{1/3}Nb_{2/3})O_3$-$xPbTiO_3$ (PMN-xPT) single crystals with $x = 0.32$. These lamellas are naturally formed in single crystals cooled under bias electric field applied along $[001]_{pc}$ and then zero-field heated to the vicinity of the so-called depoling temperature T_{RT}, but similar structures were also encountered at ambient conditions. The polarization dependence of the Raman scattering intensities was employed to demonstrate that these lamellar structures are composed of tetragonal-like and rhombohedral-like layers extending over macroscopic (mm) lengths. The properties and interest of these macroscopic heterophase interfaces are discussed.

DOI: 10.1103/PhysRevB.93.064110

I. INTRODUCTION

A large electromechanical coupling constant, piezoelectric coefficient and strain level of poled $Pb(Mg_{1/3}Nb_{2/3})_{1-x}Ti_xO_3$ (PMN-xPT) and similar single crystals have attracted considerable interest because of their excellent performance in various solid state electromechanical sensors and actuators [1–3]. It is well understood that the piezoelectricity results from the ferroelectric ordering and that the best piezoelectric figures of merit are found in materials with compositions at the so-called morphotropic phase boundary (MPB)—a boundary separating stability domains of rhombohedral-like titanium-poor phase ($x \lesssim 0.33$) from the tetragonal-like titanium-rich ($x \gtrsim 0.33$) phase in the temperature-concentration phase diagram of the material [3]. This phase boundary is only very weakly temperature dependent, but in a narrow concentration region around $x \approx 0.33$ (which precisely comprises the materials of technological interest), one may typically pass from the rhombohedral-like phase to the tetragonal-like phase at a certain [4] temperature T_{RT}, i.e., one may cross the MPB also upon heating.

Typically, to achieve high piezoelectric figures of merit, one uses rhombohedral-like material poled in a strong electric field applied along $[100]_{pc}$ direction (i.e., by a frustrative [5] poling, which favors several ferroelectric domain states at a time [1,6]). When such poled single crystals are heated above the T_{RT} temperature, their ferroelectric domain structure imposed by the frustrative poling is destroyed, and their macroscopic piezoelectric properties are degraded. Therefore, numerous efforts have been undertaken to increase the T_{RT} temperature (often denoted as *depoling* temperature) [3].

In these materials, the rhombohedral-like phase has actually a very complicated micro- and nanoscale domain texture. In fact, it is usually described as a lower symmetry phase, most often as monoclinic Cm (also denoted as M_A) and monoclinic Pm (also denoted as M_C), or even as a fine mixture of several phases of different symmetry [3,6–12].

The phase coexistence in the PMN-xPT materials close to MPB has been inferred for example from the inspection of the single crystal diffraction data [13] or from high-resolution electron microscopy studies of PMN-xPT ceramics [14]. Such experiments suggest that tetragonal-like and rhombohedral-like phases coexist at nanometer scales. However, the case of ferroelectric MPB materials is even more complicated as the chemical composition acts as an additional thermodynamical degree of freedom [15,16]. It is not quite clear whether such nanoscale ferroelectric domains are also associated with nanoscale composition fluctuations or grain boundaries. Moreover, it is not obvious whether the imaged nanodomain structures are actually the most relevant and most stable ones. Therefore, it is very interesting to investigate also *macroscopic* heterophase interfaces.

Here we have investigated the passage across the T_{RT} temperature in a PMN-0.32PT single crystal, and, in the course of these investigations, we have observed formation of *macroscopic* lamellar pattern, revealing an array of planar interfaces between the rhombohedral-like and tetragonal-like areas, or, in other words, interfaces that could be denoted as "morphotropic" interphase boundaries. The optical observation has been complemented by local-probe polarized Raman spectroscopy investigations which allowed us to distinguish between the two phases.

II. EXPERIMENT

The first sample was a 0.5-mm-thick platelet of PMN-0.32PT single crystal [17] with main facets perpendicular to the $\langle 100\rangle_{pc}$ directions. These facets were covered by evaporated gold electrodes. Optical observations and Raman scattering experiments were performed in a reflection geometry from an optically polished $(001)_{pc}$ facet [perpendicular to the principal $(100)_{pc}$ facet, see Fig. 1(b)]. Additional measurements were done with 1-mm-thick platelets of PMN-0.32PT single crystals poled in $[100]_{pc}$ and $[111]_{pc}$ directions [18].

For Raman scattering investigations, we have used a Renishaw RM 1000 micro-Raman spectrometer with a 514.5 nm Ar laser excitation line. Samples were placed into a Linkam TS 1200 high temperature cell where they were heated above the phase transition temperature. The design of the cell allows applying an electrical field to the sample, so that both the electrical field and the temperature were controlled

*hlinka@fzu.cz

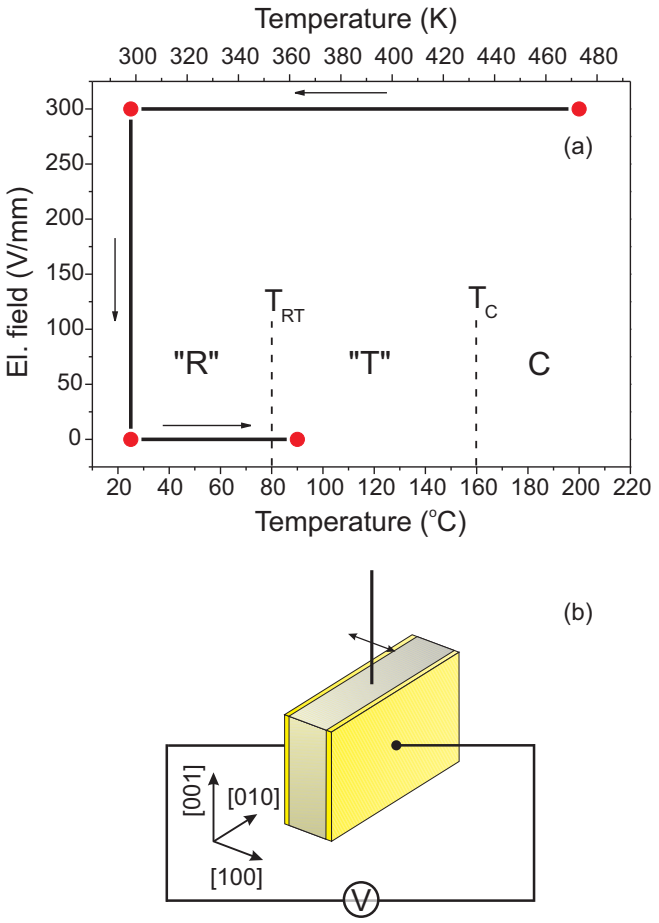

FIG. 1. Experimental arrangements used to prepare the laminate structure. (a) Schematic temperature vs $[100]_{pc}$ electric-field phase diagram with thermodynamic trajectory showing the adopted ZFHaFC experimental protocol. (b) Sketch of the experimental geometry allowing *in situ* Raman scattering or optical microscopy imaging of a facet perpendicular to the applied electric field.

during the experiment. The cell was mounted on a rotary microscope stage allowing for manual alignment of the sample with respect to the incident light polarization direction. With this experimental setup, we could use the same microscope objective for Raman scattering as well as for optical imaging *in situ*.

III. RESULTS

Prior to the Raman scattering measurement, the sample was field cooled (5 K/min) from the annealing temperature of about 470 K under a bias electric field of about 300 V/mm. This thermal treatment was done with a sample already mounted in the optical cell, but up to this point we did not observe any obvious domain contrast in our experimental arrangement. Then the electric field was removed and the sample has been driven to about 360 K [again at about 5 K/min, see Fig. 1(a)]. At this temperature we could repeatedly observe the formation of a system of roughly parallel, 10–100 μm thick stripes running across the sample at about 45 deg to the edges of the observed facet, as shown in Fig. 2.

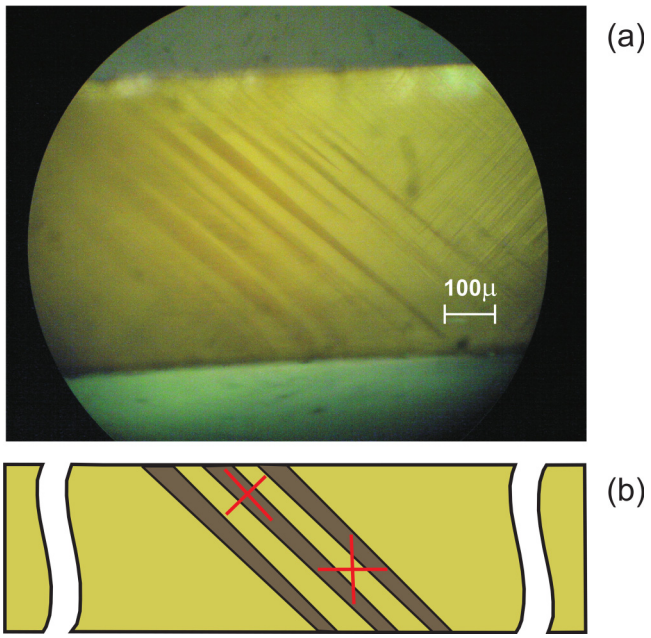

FIG. 2. Macroscopic stripe pattern formed in a PMN-0.32PT crystal after the ZFHaFC process sketched in Fig. 1. (a) Optical micrograph in a reflection mode and (b) schematic illustration. Red crosses indicate orientation of polarizers on incident and scattered beam in configurations with a minimum Raman intensity at 570 cm^{-1}.

At first sight, these images are strongly reminiscent of the observations of usual ferroelastic domains [12], but we shall argue that here, in fact, the light and dark areas correspond alternatively to lamellas of tetragonal-like and rhombohedral-like areas, respectively. Obviously the boundaries between such areas are similar to the usual ferroelastic domain boundaries. In particular, the elongated wedge shape of the observed interfaces indicates that the interfaces separate areas with different spontaneous strain tensors, which may happen at the twin boundary as well as at an interphase boundary. However, we have found that these stripes are formed only in the vicinity of the anticipated T_{RT} temperature for this composition [3,4,19,20].

To confirm this conjecture, we have investigated the nature of these stripes by polarized Raman spectroscopy. In general, it is known that Raman spectra of these materials change only slightly at ferroelectric phase transitions. In fact, the positions and shapes of the principal Raman bands in our experiments were very similar to those reported in previous investigations of PMN-xPT of a comparable composition [21–29]. Fortunately, at least the relative intensities of Raman spectra taken in dark and light stripes are different. In the following, we will report Raman spectra in the cross-polarized (HV) geometry, for which the differences were most apparent.

Spectra from selected dark and light stripes are shown in Fig. 3(a). The difference in intensity is most obvious when comparing the shape and overall intensity of the phonon bands near 600 or 800 cm^{-1}. The difference can be quantified using ratios of intensities between different bands. For example, the ratio I_{570}/I_{510} of the cross-polarized Raman intensity detected at 570 cm^{-1} with respect to that detected at 510 cm^{-1} varies by more than 50% when comparing dark and light stripes,

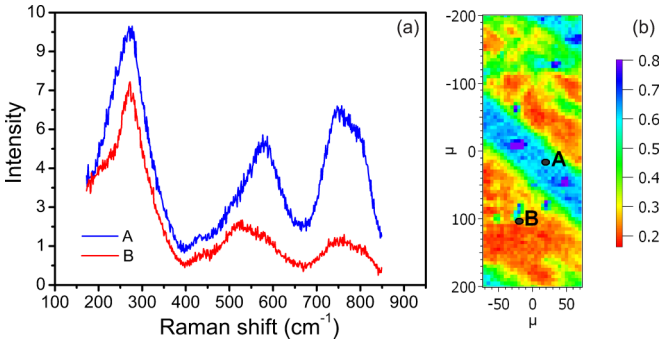

FIG. 3. Micro-Raman study of the stripe pattern of a PMN-0.32PT single crystal prepared by ZFHaFC process sketched in Fig. 1(a). (a) Cross-polarized $[z(xy)z]$ Raman spectrum of a PMN-0.32PT single crystal taken from spots (A) and (B) within dark and light stripes, respectively. (b) Map of the I_{780}/I_{270} ratio of the cross-polarized Raman scattering intensities recorded at 780 and 270 cm^{-1} reveals the stripe pattern. (The edges of the imaged area are parallel to the pseudocubic crystal axes and to the sample edges as well.)

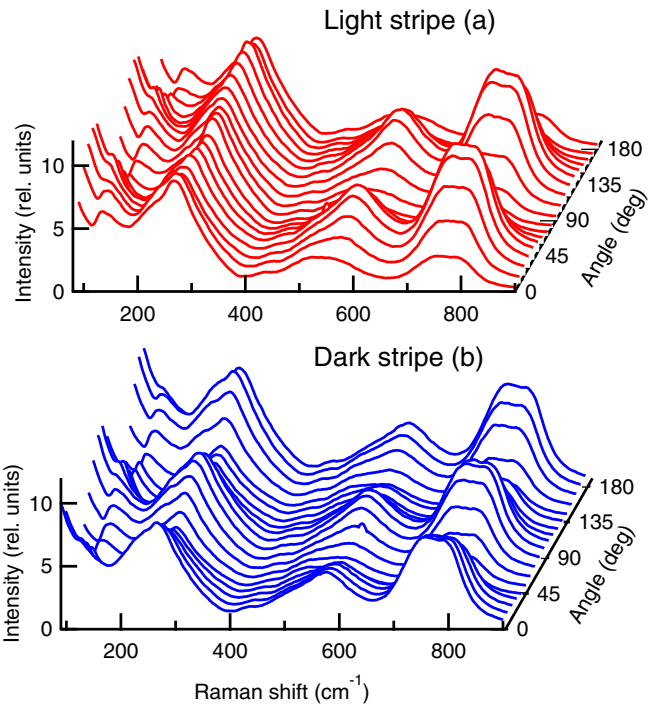

FIG. 4. Cross-polarized backscattering Raman spectra of a PMN-0.32PT single crystal prepared by ZFHaFC process sketched in Fig. 1(a), taken from a light (a) and dark (b) stripe, respectively, at varying positions of the polarizer axis (the indicated angle ϕ defines the direction of polarizer axis with respect to pseudocubic axes of the crystal; for $\phi = 0$, the polarizers are parallel to the pseudocubic crystal axes and sample edges). The angular dependence suggests that the light and dark stripes correspond to tetragonal-like and rhombohedral-like ferroelectric structural variants, respectively.

and similar contrast is obtained when considering the ratio I_{780}/I_{270} of intensities at 780 and 270 cm^{-1}. Note that both these ratios were previously used in Ref. [30] to distinguish two types of coexisting structural "microregions" of irregular shape in PMN-0.33PT, assigned to the M_A (i.e., rhombohedral-like phase) and M_C (i.e., tetragonal-like phase). We used the latter ratio to map the stripes and observed that in contrast to the results of Ref. [30], in our sample the relative intensity map obtained in this way reveals clear, about 100 μm sized stripes, which clearly match the stripes observed optically [Fig. 3(b)].

To clarify the origin of the Raman contrast associated with the stripes observed, we have recorded the variation of the Raman spectra in a given stripe as a function of the angle ϕ between the polarizer and pseudocubic crystal axes, parallel to the edges of the sample. Two sets of spectra collected from a laser spot focused within a dark and light stripe, respectively, are shown in Fig. 4. The angular dependence of Raman intensity recorded in the dark area is typical of the rhombohedral-like phase of PMN-xPT crystals (with maxima at $\phi = n\pi/2, n = 0,1,2,\ldots$), but also other rhombohedral ferroelectric crystals like $Pb(Sc_{1/2}Nb_{1/2})O_3$ [31] and it also agrees with the measurements of pure PMN, documented for example in Ref. [32]. In contrast, the angular dependence of Raman intensity recorded in the brighter areas shows the opposite behavior—positions of the intensity maxima are shifted by about 45 deg with respect to that of the dark areas (see Fig. 5).

Such angular shift cannot be simply explained by measurement in a different domain of the same rhombohedral phase: all possible Raman tensors of inequivalent rhombohedral ferroelastic domain states can be obtained by rotation around the fourfold axis parallel to the [001] direction (i.e., by a 90 deg shift in ϕ, not by a 45 deg shift in ϕ). Also, the case of a mechanically compatible tetragonal domain pair is not compatible with the relation of the recorded angular dependence of Raman intensity in the adjacent stripes: tetragonal domain states adjacent to a $(110)_{pc}$-like twin boundary should be also related by rotation around the fourfold axis parallel to the $[001]_{pc}$ direction, i.e., again by 90 deg in the angle ϕ. This argument also excludes the possibility to interpret our observation as being due to the ferroelastic domain walls between monoclinic domains of a single slightly

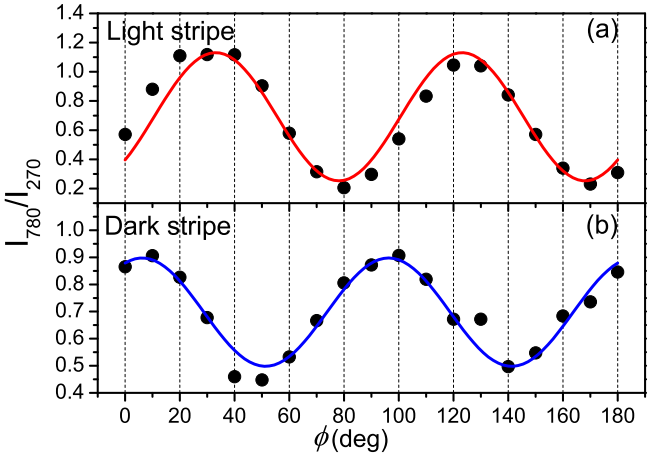

FIG. 5. Angular dependence of the I_{780}/I_{270} ratio relating the cross-polarized Raman scattering intensities recorded at 780 and 270 cm^{-1}, evaluated from data of Fig. 4. Panels allows us to compare (a) data taken in light stripe and (b) data taken in the dark stripe. Full lines are guides to the eye.

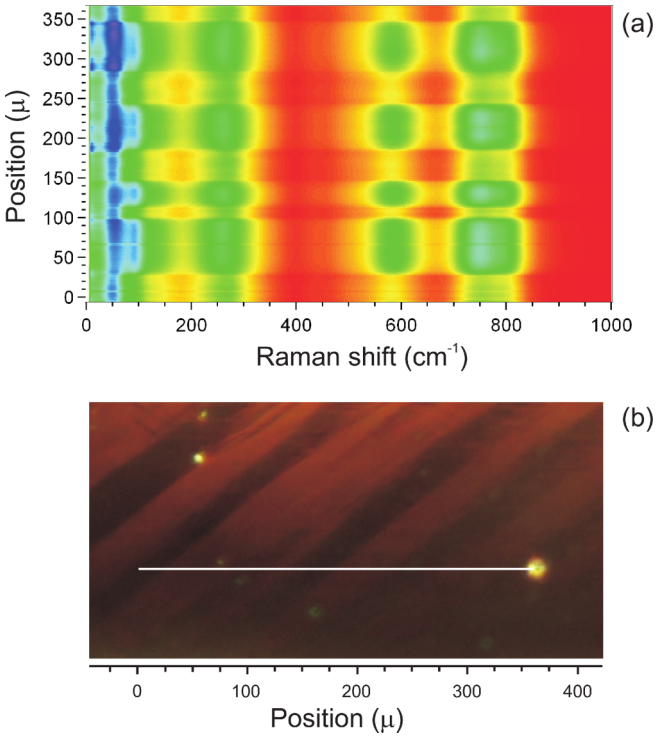

FIG. 6. Macroscopic stripe pattern observed at ambient conditions in a PMN-0.32PT crystal rapidly quenched from a state similar to that shown in Fig. 2. (a) Polarized Raman intensity as a function of Raman shift and a position along the Raman measurement trajectory, indicated by straight line in the optical micrograph (b). Polarizer and analyzer were both parallel to the $[100]_{pc}$ poling direction. The optical micrograph is taken in a reflection mode.

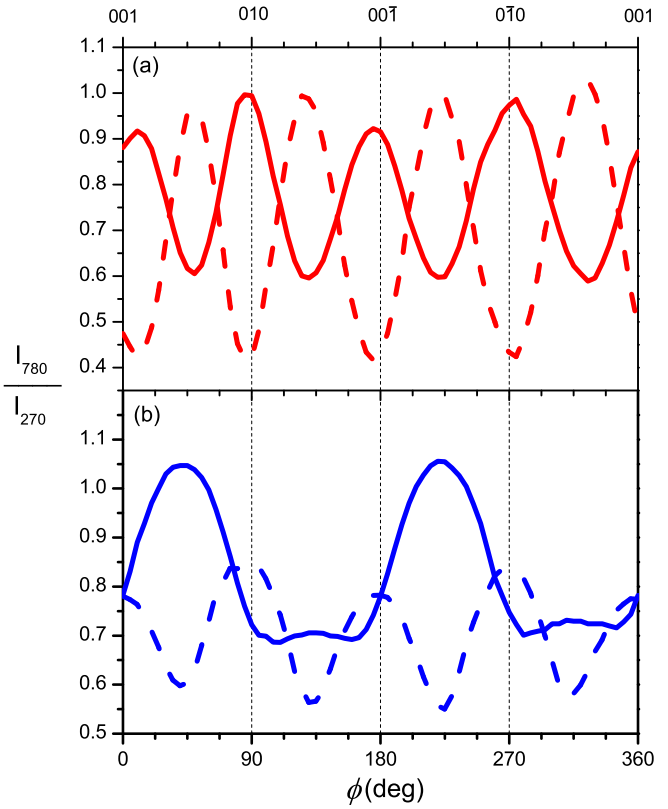

FIG. 7. Angular dependence of the intensity ratios I_{780}/I_{270} for the parallel-polarized (full lines) and cross-polarized (dashed lines) Raman scattering intensities, evaluated from the measurements taken at ambient conditions. Panels show (a) data taken in a light stripe and (b) data taken in a dark stripe of the structure shown in Fig. 6.

distorted rhombohedral ferroelectric phase alone. Similarly, it also excludes the scenario of ferroelectric domains in a monoclinic phase, structurally very close to the tetragonal one. On the contrary, $[001]_{pc}$ projections of the optical axis of one rhombohedral (or almost rhombohedral) domain and one tetragonal (or almost tetragonal) domain are always mutually at 45 deg (or almost 45 deg) apart. Therefore, the observed angular shift corroborates well the anticipated two-phase picture.

After completing the above described investigations, we have realized that fast quenching of the sample sometimes allows us to maintain the laminar structure even at room temperature. An example of such a quenched structure is shown in Fig. 6. A dense sequence of Raman spectra was taken along a line passing across the visually observed stripes. The Raman spectra are similar to those taken near 360 K, with a clear difference between the light and dark stripes. In addition, the Raman spectra for both the cross-polarized and parallel-polarized spectra were detected separately in a dark stripe and a light stripe area as a function of the angle ϕ at 5-deg steps. The angular dependence of the I_{780}/I_{270} ratios shown in Fig. 7 is very similar to that of the measurements shown in Figs. 4 and 5, taken slightly above the T_{RT} temperature.

This suggests that the tetragonal-like state can be occasionally maintained at least down to room temperature. Conversely, we have sometimes seen some residual dark stripes also well above the T_{RT} temperature, but their area (thickness) was always substantially reduced on passing around the T_{RT} temperature, which can be considered as a signature of the rhombohedral-like nature of the dark-stripe area.

It is worth noting that the angular dependence of I_{780}/I_{270} intensity ratio for the parallel-polarized Raman scattering intensities in the dark stripe [Fig. 7(b)] is completely maximized when the polarizers are parallel to the $[011]_{pc}$ direction (polarizers perpendicular to the stripes in Fig. 6), while it has only a weak local maximum near the $[01\bar{1}]_{pc}$ direction (polarizers parallel to the stripes in Fig. 6). This marked difference between dark-stripe Raman spectra polarized parallel and perpendicular to the $[011]_{pc}$ direction is also found for the I_{570}/I_{510} intensity ratio [see Fig. 8(a)]. Similarly, the parallel-polarized I_{570}/I_{510} intensity ratio is markedly different when polarizers are parallel to the $[100]_{pc}$ and $[010]_{pc}$ directions, respectively [see Fig. 8(d)].

Moreover, the parallel-polarized intensity ratios in Figs. 7(b), 8(a), and 8(d) are symmetric with respect to the position of its maxima. Due to the highly symmetric scattering geometry of the parallel-polarized scattering experiment, these symmetric maxima indicate orientations of the possible mirror symmetry operations of the structure within the given stripe. This is important because the presence of the macroscopic symmetry plane of the stripe implies that the macroscopic polarization of the stripe is contained in it. In case of the light stripe, the $(100)_{pc}$ plane is unlikely to be a symmetry plane

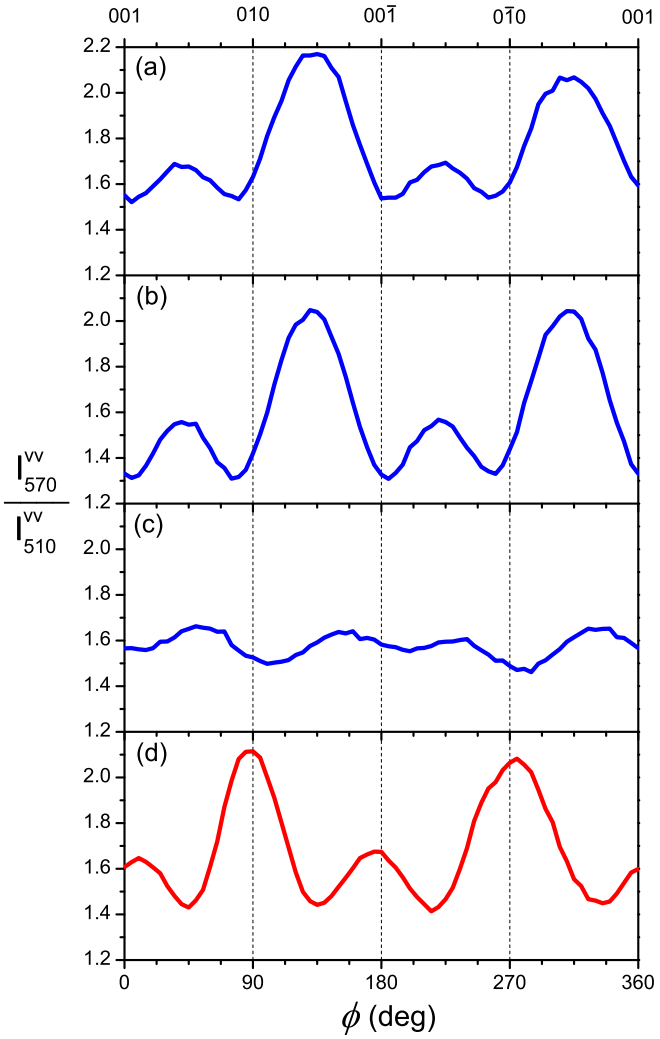

FIG. 8. Angular dependence of the I_{570}/I_{510} intensity ratio for the parallel-polarized Raman scattering intensities, evaluated from the measurements taken at ambient conditions. Panels allow us to compare (a) data taken in the dark stripe probed in Fig. 7(b), (b) data taken in a single-domain ($[111]_{pc}$-poled) sample, (c) data taken in a multidomain, frustratively poled ($[100]_{pc}$-poled) sample, and (d) data taken in the light stripe probed in Fig. 7(a). The scattering geometry with respect to the pseudocubic crystallographic axes is common to all four cases displayed.

because it is strictly perpendicular to the poling direction. However, $(010)_{pc}$ is a plausible symmetry plane there.

In order to find the orientation of the projection of the spontaneous polarization within dark stripes, we have also measured the Raman spectra of the single-domain rhombohedral PMN-32PT crystal [18]. This sample was first cut as a $[111]_{pc}$-oriented 1-mm-thick plate, poled across its thickness and then its $(001)_{pc}$ face was gently polished so that equivalent experiments could be done on this sample as well. The remarkable optical transparency of this sample testified that the sample remained in the single domain state. The angular dependence of the Raman spectra measured in the single-domain sample was very similar to that recorded in the dark stripes. For example, the I_{570}/I_{510} intensity ratio [see Fig. 8(b)] is very similar to that of the dark stripe [Fig. 8(a)].

Obviously the projection of the spontaneous polarization on the $(001)_{pc}$ viewing plane in the single domain sample is along the $[011]_{pc}$ direction. When the polarizers are parallel to it, the I_{570}/I_{510} ratio reaches the side maximum. Therefore, we can conclude that polarization of the dark stripe is perpendicular to the stripe direction.

For the sake of comparison, we have also investigated Raman spectra of the $[100]_{pc}$-oriented platelet similar to that of Fig. 2 but poled in the usual way [18], frequently employed to achieve the standard, $4mm$ symmetry multidomain state, known for the high values of the macroscopic d_{33} piezoelectric coefficient [1,6]. The angular dependence of the parallel-polarized Raman intensity ratio I_{570}/I_{510}, detected in the geometry of Fig. 1(b), is shown in Fig. 8(c). The maxima of this quantity coincide again with $[011]_{pc}$ and $[01\bar{1}]_{pc}$ directions, indicating that the sample is in the rhombohedral-like phase, as it was originally expected [1]. Moreover, the heights of all these maxima are almost equal, as can be expected for a multidomain state with equal fraction of the domain states with polarization along the $[111]_{pc}$, $[11\bar{1}]_{pc}$, $[1\bar{1}1]_{pc}$, and $[\bar{1}11]_{pc}$ crystallographic directions [6]. Summarizing, these experiments confirm that the angular dependence of the Raman scattering is capable of distinguishing clearly the rhombohedral and tetragonal phase content in PMN-xPT crystals, irrespective of the type and the macroscopic symmetry of the twinning or poling state.

IV. DISCUSSION

The present experiment gives evidence for spontaneously formed interfaces in a PMN-xPT single crystal. The interfaces separate two alternating structural variants of the same material. Many parallel interfaces are formed at a time, at 10–100 μm distances, and not just an individual phase front as encountered near the first-order phase transitions in samples under a temperature or concentration gradient [33,34].

Similar structures were possibly observed in PMN-xPT and $Pb(Zn_{1/3}Nb_{2/3})_{1-x}Ti_xO_3$ (PZN-xPT) in Refs. [35–38]. In principle, all these observations could be interpreted in terms of orientational domains of a single monoclinic phase as well as in terms of the regions belonging to two distinct phases. However, the inspection of the angular polarization profile of the Raman scattering intensity shown in this work demonstrates clearly that here we deal indeed with a *macroscopic heterophase* lamellar structure. Moreover, it was explained why the light and dark stripe regions can be associated with the tetragonal and rhombohedral phases, respectively.

The visual inspection of the observed pattern allows us to draw two additional conclusions: (i) Since the observed interphase boundaries are macroscopic *planar* objects, it can be inferred that the interfacial energy is markedly anisotropic and (ii) since, in addition, the orientation of the phase boundary with respect to the pseudocubic *crystallographic* axes is the same and reproducible, it seems obvious that its orientation is determined by elastic forces (as a prominent habit plane allowing stress-free matching of both phases).

These observations together reveal a strong analogy between the present lamellar structure and the strain-

accommodating domain structures known from studies of martensites. Several theoretical models of martensitic structures have been already proposed also for ferroelectric materials (see, e.g., Ref. [7]). The crystallographic orientation of possible low-energy mobile material interfaces in the predicted laminate structures is typically dictated by the elastic and possibly also electric compatibility of the adjacent domain states [7,39–44].

Most of the frequently studied strain-accommodating lamellar structures consist of distinct orientational variants of the *same phase*, but two-phase laminates were also proposed. The macroscopic lamellar heterophase pattern described here is reminiscent of the nanoscale lamellar heterophase patterns detected in epitaxially strained $BiFeO_3$ films [45–48]. These domain patterns have been nicely interpreted as theoretically predicted [49] lamellar structures allowing us to minimize a proper combination of the elastic, electric, and the domain interface energy (with dominant elastic contribution) [44,50].

Recently, *nanoscale* heterophase laminate structure was predicted even for PMN-xPT. According to the theoretical analysis of Ref. [51], the orientation of the predicted boundaries between the lamellas of rhombohedral and tetragonal phase is close to a {110} crystallographic plane. This is actually well compatible with the present *macroscopic* optical observations.

In addition, the same architecture of heterophase laminates can be probably encountered in single crystals of PZN-xPT. Here we refer to Fig. 7 of Ref. [35]. There is also a nicely developed system of stripes of the tetragonal-like phase, intercalated within the rhombohedral phase. According to the indicated extinction condition, it seems that the investigated PZN-xPT sample was viewed along a $\{001\}_{pc}$ direction there. This would mean that that interphase boundaries are also oriented at about 45 deg with respect to the $[001]_{pc}$ direction. Thus, the main characteristics of these heterophase stripe patterns seem to be common to both PMN-xPT and PZN-xPT systems.

Interestingly, the angular dependence recorded in the dark and light areas here are also quite analogous to that of "G microregions" and "R microregions," respectively, discovered in PMN-0.33PT single crystals by authors of Ref. [30] and then also reinvestigated in the temperature study of Ref. [52]. In contrast with our observations, the borders of the previously observed G microregions and R microregions have an irregular, spongy character. In the light of the present observations it seems quite likely that these microregions do correspond to the rhombohedral and tetragonal-like areas, even though the geometry of the boundaries of such microregions is somewhat unexpected. Different morphology is perhaps related to some frozen defects or concentration fluctuations. We also note that their PMN-0.33PT sample was studied "as-grown," whereas our observations were made with PMN-0.32PT sample and the macroscopic interphase boundaries interfaces were only observed after poling of the sample.

Finally, let us note that the nanoscale coexistence of the rhombohedral-like and tetragonal-like phases in relaxor materials with composition close to the MPB is considered as a key ingredient in the mechanism of their high piezoelectric properties [14,53–56]. It is very likely that not only the phase coexistence but mainly the architecture of the interphase boundaries is important. For example, it is possible that the phenomenon of overpoling of lead-based relaxor ferroelectric materials is related to the presence of *macroscopic* (percolated) tetragonal-like areas, while *microscopic* phase coexistence could still favor the piezoelectric response [57]. At the same time, the microscopic mechanisms responsible for the piezoelectricity in $Na_{1/2}Bi_{1/2}TiO_3$-based materials are probably very different from that of lead-based materials [58]. In either case, we believe that further studies of such heterophase boundaries are needed for understanding the functional properties of the whole family of MPB materials.

V. CONCLUSION

Our experimental observations clearly indicate that a slow zero-field heating of previously field-cooled PMN-0.32PT specimens is a protocol suitable for the stabilization of arrays of macroscopic interphase boundaries between tetragonal and rhombohedral-like (possibly monoclinic) variants of PMN-xPT single crystals. The formation of tetragonal and rhombohedral-like stripes occurs near the T_{RT} transition.

Because of their macroscopic (millimetric) size, the phase boundaries separating adjacent stripes can be easily observed in an optical microscope. In fact, the existence of a macroscopic interface boundary allowed us also to employ spatially resolved polarized Raman scattering techniques to confirm that the stripe pattern is due to the coexistence of the phases attached to the opposite sides of the morphotropic phase boundary in the temperature-composition phase diagram. However, we believe that the existence of such macroscopic interphase boundaries can be advantageous for other investigations of the coexistence and compatibility of tetragonal and rhombohedral-like (possibly monoclinic) variant MPB systems. Our results also demonstrate that MPB materials have a clear potential to sustain different interfaces than just "ordinary" ferroelectric domain walls separating two domains of the same ferroelectric phase. This might considerably enrich the domain-wall engineering opportunities available for this family of MPB crystals.

ACKNOWLEDGMENTS

This work was supported by the Czech Science Foundation (Projects 15-04121S and P204/10/0616). In addition, the contribution of I. Rafalovskyi has been supported by Czech Ministry of Education (Project SVV-2013-267303).

[1] S. E. Park and T. R. Shrout, J. Appl. Phys. **82**, 1804 (1997).
[2] D. Damjanovic, M. Budimir, M. Davis, and N. Setter, Appl. Phys. Lett. **83**, 527 (2003).
[3] S. Zhang and F. Li, J. Appl. Phys. **111**, 031301 (2012).
[4] Z. Feng, X. Zhao, and H. Luo, Solid State Commun. **130**, 591 (2004).

[5] J. Hlinka, P. Ondrejkovic, and P. Marton, Nanotechnology **20**, 105709 (2009).
[6] E. Sun and W. Cao, Prog. Mater. Sci. **65**, 124 (2014).
[7] Y. M. Jin, Y. U. Wang, A. G. Khachaturyan, J. F. Li, and D. Viehland, Phys. Rev. Lett. **91**, 197601 (2003).
[8] L. S. Kamzina, I. P. Raevskii, and E. V. Snetkova, Tech. Phys. Lett. **32**, 908 (2006).
[9] R. R. Chien, C.-S. Tu, V. H. Schmidt, and F.-T. Wang, J. Phys.: Condens. Matter **18**, 8337 (2006).
[10] J. Han and W. Cao, Phys. Rev. B **68**, 134102 (2003).
[11] In fact, a number of authors report monoclinic symmetry and fine domain pattern in the tetragonal-like phase in the vicinity of the morphotropic phase, too.
[12] A. A. Tagantsev, L. E. Cross, and J. Fousek, *Domains in Ferroic Crystals and Thin Films* (Springer, New York, 2010).
[13] C. S. Tu, C. M. Hsieh, R. R. Chien, V. H. Schmidt, F. T. Wang, and W. S. Chang, J. Appl. Phys. **103**, 074117 (2008).
[14] H. Wu, D. Xue, D. Lv, J. Gao, S. Guo, Y. Zhou, X. Ding, C. Zhou, S. Yang, Y. Yang, and X. Ren, J. Appl. Phys. **112**, 052004 (2012).
[15] W. Cao and L. E. Cross, Phys. Rev. B **47**, 4825 (1993).
[16] G. A. Rossetti, Jr., W. Zhang, and A. G. Khachaturyan, Appl. Phys. Lett. **88**, 072912 (2006).
[17] High quality crystals provided by APC International, Ltd.
[18] High quality poled crystals provided by CTG Advanced Materials.
[19] J. Peräntie, J. Hagberg, A. Uusimäki, J. Tian, and P. Han, J. Appl. Phys. **112**, 034117 (2012).
[20] E. A. McLaughlin, T. Liu, and C. S. Lynch, Acta Mater. **53**, 4001 (2005).
[21] A. Slodczyk and P. Colomban, Materials **3**, 5007 (2010).
[22] M. E. Marssi, R. Farhi, and Y. I. Yuzyuk, J. Phys.: Condens. Matter **10**, 9161 (1998).
[23] S. Kamba, E. Buixaderas, J. Petzelt, J. Fousek, J. Nosek, and P. Bridenbaugh, J. Appl. Phys. **93**, 933 (2003).
[24] B. Chaabane, J. Kreisel, P. Bouvier, G. Lucazeau, and B. Dkhil, Phys. Rev. B **70**, 134114 (2004).
[25] J. A. Lima, W. Paraguassu, P. T. C. Freire, A. G. Souza Filho, C. W. A. Paschoal, J. Mendes Filho, A. L. Zanin, M. H. Lente, D. Garcia, and J. A. Eiras, J. Raman Spectrosc. **40**, 1144 (2009).
[26] A. Slodczyk, P. Daniel, and A. Kania, Phys. Rev. B **77**, 184114 (2008).
[27] H. Ohwa, M. Iwata, H. Orihara, N. Yasuda, and Y. Ishibashi, J. Phys. Soc. Jpn. **70**, 3149 (2001).
[28] I. G. Siny, S. G. Lushnikov, R. S. Katiyar, and V. H. Schmidt, Ferroelectrics **226**, 191 (1999).
[29] M. Shen, G. G. Siu, Z. K. Xu, and W. Cao, Appl. Phys. Lett. **86**, 252903 (2005).
[30] Y. Yang, Y. L. Liu, L. Y. Zhang, K. Zhu, S. Y. Ma, G. G. Siu, Z. K. Xu, and H. S. Luo, J. Raman Spectrosc. **41**, 1735 (2010).
[31] J. Pokorny, I. Rafalovskyi, I. Gregora, F. Borodavka, M. Savinov, J. Drahokoupil, M. Tyunina, T. Kocourek, M. Jelinek, Y. Bing, Z.-G. Ye, and J. Hlinka, J. Adv. Dielect. **5**, 1550013 (2015).
[32] H. Taniguchi, M. Itoh, and D. Fu, J. Raman Spectrosc. **42**, 706 (2011).
[33] J. Bornarel and R. Cach, Phys. Rev. B **60**, 3806 (1999).
[34] V. A. Shuvaeva, A. M. Glazer, and D. Zekria, J. Phys.: Condens. Matter **17**, 5709 (2005).
[35] K. Fujishiro, R. Vlokh, Y. Uesu, Y. Yamada, J.-M. Kiat, B. Dkhil, and Y. Yamashita, Jpn. J. Appl. Phys. **37**, 5246 (1998).
[36] P. Bao, F. Yan, X. Lu, J. Zhu, H. Shen, Y. Wang, and H. Luo, Appl. Phys. Lett. **88**, 092905 (2006).
[37] G. Xu, H. Luo, H. Xu, and Z. Yin, Phys. Rev. B **64**, 020102 (2001).
[38] L. Zheng, X. Lu, H. Shang, Z. Xi, R. Wang, J. Wang, P. Zheng, and W. Cao, Phys. Rev. B **91**, 184105 (2015).
[39] A. G. Khachaturyan, S. M. Shapiro, and S. Semenovskaya, Phys. Rev. B **43**, 10832 (1991).
[40] D. Viehland, J. Appl. Phys. **88**, 4794 (2000).
[41] V. Yu. Topolov and Z. G. Ye, Phys. Rev. B **70**, 094113 (2004).
[42] V. Yu. Topolov, Phys. Rev. B **71**, 134103 (2005).
[43] S. Dorfman, D. Fuks, A. Gordon, A. V. Postnikov, and G. Borstel, Phys. Rev. B **52**, 7135 (1995).
[44] J. Ouyang, W. Zhang, X. Huang, and A. L. Roytburd, Acta Mater. **59**, 3779 (2011).
[45] R. J. Zeches, M. D. Rossell, J. X. Zhang, A. J. Hatt, Q. He, C.-H. Yang, A. Kumar, C. H. Wang, A. Melville, C. Adamo, G. Sheng, Y.-H. Chu, J. F. Ihlefeld, R. Erni, C. Ederer, V. Gopalan, L. Q. Chen, D. G. Schlom, N. A. Spaldin, L. W. Martin, and R. Ramesh, Science **326**, 977 (2009).
[46] R. K. Vasudevan, Y. Liu, J. Li, W.-I. Liang, A. Kumar, S. Jesse, Y.-C. Chen, Y.-H. Chu, V. Nagarajan, and S. V. Kalinin, Nano Lett. **11**, 3346 (2011).
[47] J. X. Zhang, R. J. Zeches, Q. He, Y.-H. Chu, and R. Ramesh, Nanoscale **4**, 6196 (2012).
[48] M. D. Rossell, R. Erni, M. P. Prange, J.-C. Idrobo, W. Luo, R. J. Zeches, S. T. Pantelides, and R. Ramesh, Phys. Rev. Lett. **108**, 047601 (2012).
[49] J. Ouyang and A. L. Roytburd, Acta Mater. **54**, 5565 (2006).
[50] W. Zhang, J. Ouyang, and A. L. Roytburd, Scr. Mater. **66**, 499 (2012).
[51] Y. Zhang, D. Xue, H. Wu, X. Ding, T. Lookman, and X. Ren, Acta Mater. **71**, 176 (2014).
[52] Y. Yang, L. Y. Zhang, K. Zhu, and Y. L. Liu, J. Appl. Phys. **109**, 083517 (2011).
[53] C. Ma, H. Guo, S. P. Beckman, and X. Tan, Phys. Rev. Lett. **109**, 107602 (2012).
[54] Y. Sato, T. Hirayama, and Y. Ikuhara, Phys. Rev. Lett. **107**, 187601 (2011).
[55] L. A. Schmitt and H.-J. Kleebe, Func. Mater. Lett. **3**, 55 (2010).
[56] M. Iwata and Y. Ishibashi, Jpn. J. Appl. Phys. **51**, 09LE03 (2012).
[57] K. K. Rajan, M. Shanthi, W. S. Chang, J. Jin, and L. C. Lim, Sensors Actuators A **133**, 110 (2007).
[58] M. Guennou, M. Savinov, J. Drahokoupil, H. Luo, and J. Hlinka, Appl. Phys. A **116**, 225 (2014).